Intermetallics xxx (2010) 1–9

Contents lists available at ScienceDirect

Intermetallics

journal homepage: www.elsevier.com/locate/intermet

First-principles phase stability calculations and estimation of finite temperature effects on pseudo-binary $Mg_6(Pd_xNi_{1-x})$ compounds

J.F. Fernandez [a,*], M. Widom [b], F. Cuevas [c], J.R. Ares [a], J. Bodega [a], F. Leardini [a], M. Mihalkovič [d], C. Sánchez [a]

[a] Departamento de Física de Materiales, Facultad de Ciencias, Universidad Autónoma de Madrid, 28049 Madrid, Spain
[b] Department of Physics, Carnegie Mellon University, Pittsburgh, PA 15213, USA
[c] CMTR/ICMPE/CNRS, UMR7182, 2-8 rue Henri Dunant, 94320 Thiais Cedex, France
[d] Institute of Physics, Slovak Academy of Sciences, 84228, Bratislava, Slovakia

ARTICLE INFO

Article history:
Received 22 June 2010
Received in revised form
18 November 2010
Accepted 19 November 2010
Available online xxx

Keywords:
A. Intermetallics, miscellaneous
B. Thermodynamic and thermochemical properties
B. Phase diagrams
E. Electronic structure, calculation
G. Hydrogen storage

ABSTRACT

The stability of pseudo-binary $Mg_6(Pd_xNi_{1-x})$ compounds has been studied at $T = 0$ K via first-principles calculations and at 673 K by thermodynamic modelling of finite temperature effects. At 0 K, these compounds are not stable since their formation energy is above the convex hull defined by the Mg, Mg_2Ni and Mg_6Pd phases, although the energy difference is not very high. However, at 673 K, vibrational and configurational entropic effects allow the stabilisation of some of the calculated pseudo-binary $Mg_6(Pd_xNi_{1-x})$ compounds. The vibrational contribution to the thermodynamic properties of the studied compounds has been calculated from Debye temperatures in the harmonic approximation. Also, the configurational entropy has been estimated taking into account the possible distribution of Pd and Ni between the several sites available in the pseudo-binary structure. The identification of intrinsic disorder and the associated energies and entropy are innovative features of this work. The phase diagram at the Mg-rich corner derived from these calculations is in fairly good agreement with recently published experimental results. In addition, the Ni for Pd substitution has been studied for the several sites available for Pd in the binary Mg_6Pd compound. The calculated preferential site occupancy is in agreement with the site occupancy factors determined in recent neutron diffraction experiments.

1. Introduction

The quest for new light alloys with good hydrogen (H) storage properties, i.e., high gravimetric and volumetric H content, fast H-diffusion and able to work reversibly at mild conditions of temperature and pressure, is a very important goal for the future development of the H-economy [1]. Mg metal with very high specific and volumetric hydrogen capacities (7.6 wt.% H and 108 gH_2/l, respectively) is one of the more interesting materials to achieve such a goal, although it suffers from slow kinetics and its hydride is too stable for practical applications [2,3]. In the last few decades, a systematic investigation of Mg-based binary compounds has been undertaken [4–8] with the objective of finding new hydrides less stable than MgH_2. A general conclusion from these investigations is that the observed destabilisation is small. On the other hand, Mg-ternaries remain a largely unexplored field. This is due, on the one hand, to the large number of possible combinations available out of three elements and, on the other hand, to the limited determination and reliability of the existing ternary phase diagrams. To this aim, computational approaches, like the CALPHAD method [9,10], are of great help on predicting the stability and phase boundaries of complex systems. This method requires the use of model parameters that are usually assessed from experiments, being limited by the possibility to perform such experiments. On the other hand, first-principles calculations can provide the basic data needed for the CALPHAD modelling in this way improving its usefulness.

Recently, we have started a research activity on the phase stability and hydrogenation properties of pseudo-binary $Mg_6(Pd_xNi_{1-x})$ Mg-rich intermetallic compounds (IMCs) [11–14]. We have shown that the Ni solubility limit in these compounds attains 9 at. % Ni at 673 K. This finding was unexpected as the previous assessment of the ternary Mg–Ni–Pd phase diagram at 673 K reported that Ni solubility in the Mg_6Pd phase only extends up to 2 at. %Ni [15]. The crystal structure of these compounds is the same as for the cubic Mg_6Pd IMC. Neutron and X-ray diffraction indicated that Ni substitution occurs on the three crystallographic sites exclusively occupied by Pd in the Mg_6Pd phase and that is not fully random, taking mainly place

* Corresponding author. Tel.: +34914976704; fax: +34914978579.
E-mail address: josefrancisco.fernandez@uam.es (J.F. Fernandez).

0966-9795/$ – see front matter © 2010 Elsevier Ltd. All rights reserved.
doi:10.1016/j.intermet.2010.11.024

in sites with a low coordination number. The unit cell composition at the Ni solubility limit is $Mg_{344(2)}Pd_{12(1)}Ni_{36(1)}$ with 75% of Ni atoms substituting Pd ones [14]. More structural information (Wyckoff positions, atomic coordinates, site occupancy factors and so on) can be obtained elsewhere [11].

The binary compound Mg_6Pd belongs to a family of cubic complex intermetallic compounds, Mg_yX (with a Mg:X atomic ratio in the range 6:1–7:1) in which X is a late transition metal atom. Some stable members of the family are $Mg_{29}Ir_4$ [16], Mg_6Pd [17], Mg_6Pt [18], $Mg_{44}Rh_7$ [19] and $Mg_{44}Ru_7$ [20]. The Mg_6Ni intermetallic compound has also been obtained as a metastable phase either by high pressure means [21] or by crystallization of melt-spun amorphous ribbons [22,23]. It decomposes into Mg and Mg_2Ni on heating above ~500 K. The Mg_6Ni phase is especially attractive for H_2-storage due to its expected high gravimetric density and, also, to the good catalytic properties of Ni for H_2 dissociation.

In this paper we report on the stability of the pseudo-binary $Mg_6Pd_xNi_{1-x}$ IMCs as determined from Gibbs free energy considerations. We study the compound without hydrogen both as a first step, and because its stability without hydrogen is both interesting and important. To this aim, the enthalpy of formation of all experimentally known stable and metastable Mg–Ni–Pd structures at the Mg-rich corner of the ternary phase diagram is evaluated from first-principles calculations at $T = 0$ K (Section 3.1) and the thermodynamics at finite temperature of 673 K is determined from an estimation of the Debye temperature of the IMCs (Section 3.2). The method is validated in Section 3.2.1 by comparing the vibrational enthalpy and entropy obtained by the Debye model and phonon calculations for some simple structures studied in this work (Mg.hp2, Mg2Ni.hp18) and also in the most symmetric structures ($Mg_{348}Pd_{48}$.cF412 and $Mg_{348}Ni_{48}$.cF412) of the complex compounds. From these results, we have described with good accuracy the phase diagram of the ternary Mg–Pd–Ni system at the Mg-rich corner, despite the complexity of some of the compounds involved in the calculations such as the pseudo-binary $Mg_6(Pd_xNi_{1-x})$ IMCs with almost 100 atoms in the primitive cell. The identification of intrinsic disorder and the associated energies and entropy are innovative features of this work.

2. Theory

2.1. Phase stability at $T = 0$ K

Our first-principles calculations employ electronic Density Functional Theory (DFT) as implemented in the plane-wave program VASP [24,25]. Projector augmented wave potentials [26,27] were used in the PW91 generalized gradient approximation [28]. We use normal precision FFT grids which allow for small wrap-around errors, and default energy cutoffs (i.e., the highest default value for the elements present). PAW potential valences and energy cutoffs are: Mg, $Z = 2$, 210 eV; Pd, $Z = 10$, 251 eV; Ni, $Z = 10$, 270 eV. We checked that holding the energy cutoff fixed at 300 eV makes no significant difference. All atomic coordinates and cell parameters are fully relaxed and k-point meshes refined following procedures as described in [29] until total energies are converged to within 1 meV/atom. In particular k-point meshes require linear k-mesh densities (divisions divided by reciprocal lattice vector) exceeding 40 Å. Because all atomic coordinates have been relaxed, the calculated total energy corresponds to a state at $T = 0$ K. Since all cell parameters have been relaxed, the energy corresponds to an enthalpy at $P = 0$ GPa.

We subtract all our total energies from a tie-surface joining the energies of the pure elements and thus we report $T = 0$ K, $P = 0$ GPa enthalpies of formation. The convex hull of enthalpy as a function of composition predicts the $T = 0$ K phase diagram. We carry out calculations for all known crystal structures and several hypothetical ones as well, in order to test the reliability of our calculations. Complete ab-initio data can be found on the web [30]. Perfect agreement between theory and experiment requires that all known metastable, high temperature and hypothetical structures lie above the convex hull. All known low-temperature stable structures must lie on vertices of the convex hull.

A byproduct of our density functional calculations is the electronic density of states. For both Mg_6Ni and Mg_6Pd, the density of states resembles a free-electron parabola with a narrow d-band superimposed, and also with a weak pseudogap just below the Fermi energy. The Pd d-band lies further below the Fermi energy than the Ni d-band. Otherwise the densities of states resemble each other.

2.2. Phase stability at finite temperatures

All compounds at the Mg-rich corner of the Mg–Pd–Ni phase diagram studied in this work, apart from the elements and Mg_2Ni, are complex IMCs with a huge number of atoms in the unit cell. This implies that the calculation of their vibrational properties from first-principles is a quite demanding task. To circumvent this problem, we have implemented a thermodynamic model which takes into account vibrational and configurational effects as the main contribution to the finite temperature thermodynamics. The method has been validated by performing phonon calculations for simple structures like Mg.hp2 and Mg_2Ni.hp18 and, also, for the most symmetric complex compounds, $Mg_{348}Pd_{48}$.cF412 and $Mg_{348}Ni_{48}$.cF412.

To calculate the vibrational properties of the compounds, the harmonic approximation was used, characterised by the low-temperature limit of the Debye temperature, θ_0, of the compounds. Specific heat, enthalpy and entropy as a function of temperature can be deduced from the knowledge of θ_0 and values of the enthalpy at $T = 0$ K.

Calculation of θ_0 for a compound is usually made by relating this temperature to some function of the elastic constants of the material [31]. A simplification of such a method allows writing a relationship between θ_0 and the elastic modulus G_c, which, in turn, is calculated from the elastic constants in a well defined way. The equation used in our work is a further simplification needed when the elastic constants for the compounds are unknown. We replace the elastic modulus G_c with the bulk modulus B_0, a parameter much easier to compute. According to previous work [32,33] that replacement is accurate within an error limit of approximately 15%.

We have started by obtaining the bulk modulus at $T = 0$ K (B_0) following a method that correlates B_0 and atomic properties of binary and ternary intermetallics [34,35].

$$B_0 = \eta_{WS} V \left[1 + \frac{\Delta H}{E_{coh}}\right] \quad (1)$$

where η_{WS} and V are the valence electron density and molar volume of the compound, whereas ΔH and E_{coh} are their formation enthalpy and cohesive energy, respectively. Eq. (1) predicts B_0 values of binary and ternary intermetallic compounds with an average error limit of ±11% and ±8.5% respectively.

When available, the molar volume V was obtained from experimental lattice parameter data. Otherwise, the lattice parameters obtained from first-principles calculations were used. Values of η_{WS} were calculated from a weighted formula taking into account η_{WS} and V values for the elements and the molar volume of the intermetallic compound.

Moruzzi et al. [36] have proposed a direct correlation between θ_0 and B_0 for cubic crystals. Later on, Chen and Sundman [37] criticised the model and extended it for hexagonal structures.

Please cite this article in press as: Fernandez JF, et al., First-principles phase stability calculations and estimation of finite temperature..., Intermetallics (2010), doi:10.1016/j.intermet.2010.11.024

The method is based on expressions relating the longitudinal and transverse modulus to the bulk modulus and Poisson ratio which allows writing a simplified expression for θ_0.

$$\theta_0 = k(\nu)\frac{\hbar}{k_b}\left(\frac{6\pi^2 N_a \rho}{M}\right)^{1/3}\sqrt{\frac{B_0}{\rho}} \quad (2)$$

where N_a is the Avogadro number, ρ the IMC density, M the weighted arithmetical average of the masses of the atoms composing the IMC, $k(\nu)$ the Poisson ratio, $\hbar$ the Planck constant over 2π and k_b the Boltzmann constant. $k(\nu)$ is essentially constant for compounds crystallising in the same crystal system, allowing calculation of θ_0 from the much accessible knowledge of B_0. We have used $k(\nu)$ values of 0.617 and 0.810 for cubic and hexagonal systems, respectively [36,37].

The configurational entropy should be considered for compounds in which Ni for Pd substitution takes place and also to take into account the homogeneity range of the binary Mg_6Pd phase. The origin of the homogeneity range of the binary Mg_6Pd phase comes from the substitution of Mg by Pd in site N^0 12 (we follow the notation used in [17], see Table 2 later on). As for the pseudo-binary $Mg_6(Pd_xNi_{1-x})$ [11], Ni substitute for Pd in each site available for Pd, i.e., the sites N^0 10, 11, 12 and 13. However, the amount of Ni found in site 12 is very reduced (fractional occupancy $\leq$0.04) and then for the present calculations we assume this site is only occupied by Mg and Pd. We disregard other small contributions to the configurational entropy such as constitutional Mg vacancies that, in a small number, appear in the structure [17,38]. Therefore, the configurational entropy is calculated by assuming four sublattices in which random substitution of Ni for Pd or Pd for Mg can take place.

$$S^{conf} = -\frac{R}{4}\sum_{i=1}^{3}(y_i \ln y_i + (1-y_i)\ln(1-y_i)) - \frac{R}{4}(y_4 \ln y_4 + (1-y_4)\ln(1-y_4)) \quad (3)$$

where R is the gas constant, y_i is the Ni to Pd fraction in site i (site 10,11 or 13) while y_4 is the Mg to Pd fraction in site 12.

2.2.1. Phonon calculations

Phonon calculations are performed in the ab-initio force-constant approach [39] using density functional perturbation theory to calculate the Hessian matrix, as implemented in VASP version 5.2. To minimize interactions of atoms with their repeated images, we employ supercells with edge lengths exceeding 13 Å. For Mg_6(Ni, Pd) only the primitive cell was required. We convert the Hessian into a dynamical matrix at k-points on a reciprocal space grid within the first Brillouin zone and obtain eigenvalues using a standard LAPACK routine. Gaussian smearing of width $\sigma = 0.05$ THz produces a continuous density of states. Our k-point mesh densities exceed 60 Å in each linear dimension. For Mg and Mg_2Ni we checked that these supercell and k-mesh criteria result in well-converged densities of states. Our density of states for Magnesium is in excellent agreement with the experimental determination [40].

The harmonic vibrational Gibbs free energy at finite temperature was calculated from the following relationship [41]

$$G^h_{vib}(T) = RT\int_0^\infty \ln\left[2\sinh\left(\frac{h\nu}{2k_bT}\right)\right]g(\nu)d\nu \quad (4)$$

where h is the Plank's constant, k_b the Boltzmann's constant, ν the frequency and $g(\nu)$ the phonon density of states, normalised to three per atom.

3. Results and discussion

3.1. First-principles calculations at T = 0 K

Table 1 summarizes information for all compounds calculated in this work. The structures are labelled by giving either the chemical formula, for stoichiometric compounds, or the number of atoms in the unit cell, for the non-stoichiometric ones, followed by the Pearson structure symbol.

3.1.1. Lattice parameters

The calculated lattice parameter is compared, when available, to experimental results at RT (Data obtained from [23,38,42–44] and PDF files). As can be seen reasonable agreement between both quantities is found. For the binary Mg_6Pd phase, the lattice parameter decreases with the decrease in Mg content (N^0 7 to 14 in Table 1), as expected from the higher metallic radii of Mg (r_{Mg} = 1.60 Å) as compared to Pd (r_{Pd} = 1.37 Å). Similarly the substitution of Ni for Pd produces a drastic reduction of the lattice parameter as can be seen by comparing both, the two binaries (N^0 7 with N^0 6), and the pseudo-binaries (N^0 19 to 23), although in the latter case the Mg content plays a more important role than the Ni to Pd fraction. Again this can be explained as due to the larger atomic radii of Pd compared to Ni (r_{Ni} = 1.23 Å).

3.1.2. Mg–Ni binary formation enthalpies

Last two columns of Table 1 give the formation enthalpy, Δ_fH_0, and the energy distance to the convex hull, ΔE. The ΔE parameter is positive for structures above the convex hull. The structures belonging to the convex hull are labelled as stable in Table 1.

For the Mg–Ni binary we obtain perfect agreement with the accepted phase diagram [45], with Mg_2Ni.hP18 and $MgNi_2$.hP24 on the hull and $Mg_{348}Ni_{48}$.cF412 lying above. Fig. 1a displays the calculated Δ_fH_0 for the Mg–Ni binary phase diagram. Crosses stand for the Δ_fH_0 of calculated compounds while the solid line is the tie-line formed by stable compounds: Mg.hP2, Mg_2Ni.hP18 and $MgNi_2$.hP24. The Δ_fH_0 of Mg_2Ni.hP18 agrees well with previously published values, −20.1 [46] and −21.8 [47] kJ/mol-atom. We correctly identify $Mg_{348}Ni_{48}$.cF412 as an unstable compound, with a ΔE value of 0.77 kJ/mol-atom from the tie-line. Note that the ΔE value is not very high so we can expect metastability for this compound.

3.1.3. Mg–Pd binary formation enthalpies

The Mg–Pd binary phase diagram is highly complex [38]. The large number of compounds in this system compared to those in the Mg–Ni one is an indication of stronger interaction between Mg and Pd atoms compared to Mg and Ni atoms. Δ_fH_0 for compounds at the Mg-rich part of the Mg–Pd phase diagram is shown in Fig. 1b. Symbols have the same meaning as in Fig. 1a. The reported compounds stable at low-temperature, $Mg_{348}Pd_{48}$.cF412, Mg_3Pd.hP24, Mg_5Pd_2.hP28 and MgPd.cP2, all lie on the convex hull. We also have found $Mg_{57}Pd_{13}$.cP140 to be stable though experimentally it might be only stable above 807 K [38]. The formation enthalpy decreases with the decrease in Mg content from −22.7 kJ/mol-atom for $Mg_{348}Pd_{48}$.cF412, to −75.30 kJ/mol-atom for MgPd.cP2. As far as we know, except for Mg_3Pd, there are neither experimental data nor first-principles calculations for comparison. For Mg_3Pd, Deng et al. [48] have calculated a formation enthalpy of −42.4 kJ/mol-atoms in fairly good agreement with our results.

Regarding the binary and pseudo-binary Mg_6(Pd–Ni) structures, Table 2 gives a complete description of the site occupation in these structures. For the binaries (N^0 7 to 14), the increasing Pd content is taken into account by progressive substitution of Mg atoms by Pd ones in site 12. For some of them, Mg vacancies at site 14 (N^0 8 or 10) or at site 1 (N^0 12) were included.

Please cite this article in press as: Fernandez JF, et al., First-principles phase stability calculations and estimation of finite temperature..., Intermetallics (2010), doi:10.1016/j.intermet.2010.11.024

Table 1
Calculated and experimental lattice parameters of Mg–Pd–Ni structures, formation energy, $\Delta_f H_0$, and energy difference, ΔE, from convex hull at $T = 0$ K.

N[0]	Structure	Space group	DFT		Experimental		$\Delta_f H_0$ (kJ/mol-atom)	ΔE (kJ/mol-atom)
			a(Å)	c(Å)	a(Å)	c(Å)		
1	Mg.hp2	$P6_3/mmc$	3.1966	5.1764	3.2094	5.2112[a]	0.00	Stable
2	Pd.cF4	$Fm\bar{3}m$	3.9250		3.8902[b]		0.00	Stable
3	Ni.cF4	$Fm\bar{3}m$	3.4954		3.5238[c]		0.00	Stable
4	Mg_2Ni.hP18	$P6_222$	5.1974	13.1351	5.2050	13.236[d]	−20.26	Stable
5	$MgNi_2$.hP24	$P6_3/mmc$	4.8073	15.7189	4.8250	15.7900[e]	−24.27	Stable
6	$Mg_{348}Ni_{48}$.cF412	$F\bar{4}3m$	20.0059		20.02[f]		−6.60	0.77
7	$Mg_{348}Pd_{48}$.cF412	$F\bar{4}3m$	20.2009		20.1985[g]		−22.73	Stable
8	$Mg_{344}Pd_{48}$.cF412	$F\bar{4}3m$	20.1561				−22.90	0.05
9	$Mg_{344}Pd_{52}$.cF412	$F\bar{4}3m$	20.1513				−24.52	0.02
10	$Mg_{340}Pd_{52}$.cF412	$F\bar{4}3m$	20.1230				−24.06	0.71
11	$Mg_{340}Pd_{56}$.cF412	$F\bar{4}3m$	20.1025[h]				−26.32	0.02
12	$Mg_{336}Pd_{56}$.cF412	$F\bar{4}3m$	20.0524[h]				−25.39	1.22
13	$Mg_{336}Pd_{60}$.cF412	$F\bar{4}3m$	20.0387		20.045[i]		−28.10	0.05
14	$Mg_{332}Pd_{64}$.cF412	$F\bar{4}3m$	19.9809				−29.83	0.12
15	$Mg_{57}Pd_{13}$.cP140	$Pm\bar{3}m$	14.0433				−34.25	Stable
16	Mg_3Pd.hP24	$P6_3cm$	8.0279	8.3292	7.987(1)	8.422(1)[j]	−44.50	Stable
17	Mg_5Pd_2.hP28	$P6_3/mmc$	8.7148	8.1340	8.671(1)	8.164(1)[k]	−49.88	Stable
18	MgPd.cP2	$Pm\bar{3}m$	3.1729		3.1570(3)[l]		−75.30	Stable
19	$Mg_{344}Pd_{28}Ni_{24}$.cF412	$F\bar{4}3m$	20.1416		20.13331(7)[m]		−16.52	0.54
20	$Mg_{340}Pd_{32}Ni_{24}$.cF412	$F\bar{4}3m$	20.0723				−18.30	0.67
21	$Mg_{348}Pd_{32}Ni_{16}$.cF412	$F\bar{4}3m$	20.1654				−17.10	0.65
22	$Mg_{348}Pd_{32}Ni_{16}$.cF412	$F\bar{4}3m$	20.1490				−17.48	0.27
23	$Mg_{348}Pd_{32}Ni_{16}$.cF412	$F\bar{4}3m$	20.1537				−17.18	0.56

[a] PDF-00-035-0921.
[b] PDF-00-046-1043.
[c] PDF-00-004-0850.
[d] PDF-00-075-1249.
[e] PDF-00-025-1374.
[f] Atomic composition: $Mg_{339..4}Ni_{56.6}$[24].
[g] Atomic composition: $Mg_{336.6}Pd_{59.4}$[38].
[h] Small rhombohedral cell distortion. Average lattice parameter.
[i] Atomic composition: $Mg_{346}Pd_{50}$ [38].
[j] Ref. [42].
[k] Ref. [43].
[l] Ref. [44].
[m] Atomic composition: $Mg_{342}Pd_{29}Ni_{23}$ [11].

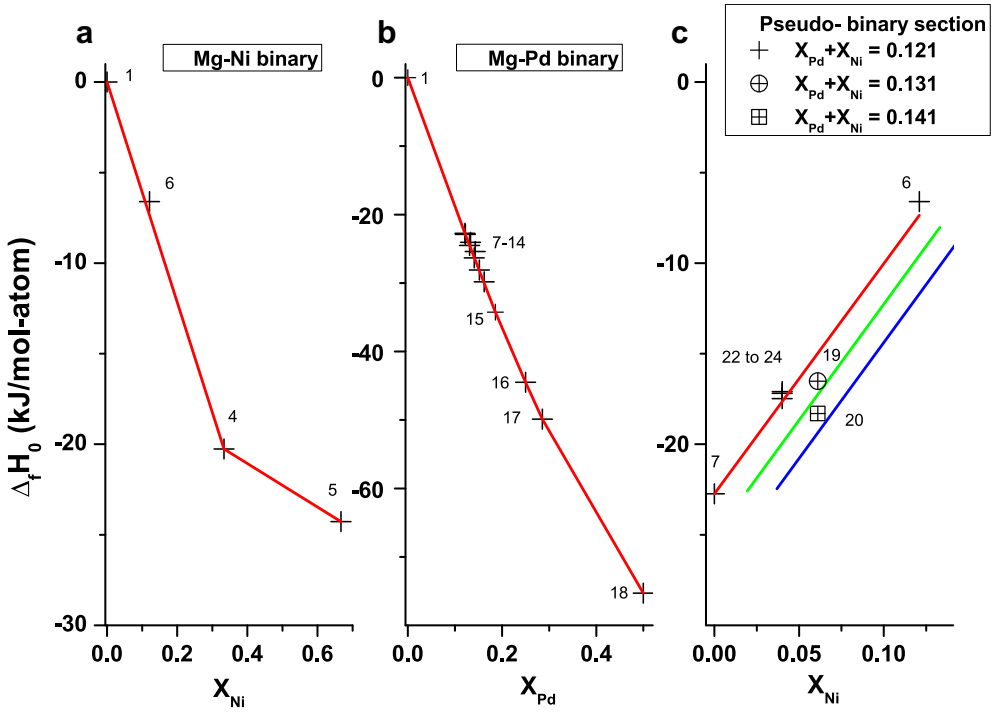

Fig. 1. a) Enthalpies of formation (crosses) and their convex hulls (solid lines) at the Mg-rich corner of the Mg–Ni phase diagram for the calculated structures. Numbers are from Table 1. b) Same for the Mg–Pd phase diagram. c) Same for pseudo-binary sections for three different Pd + Ni atomic fractions as a function of atomic Ni content.

Please cite this article in press as: Fernandez JF, et al., First-principles phase stability calculations and estimation of finite temperature..., Intermetallics (2010), doi:10.1016/j.intermet.2010.11.024

Table 2
Description of site occupation in the Mg_6(Pd−Ni) calculated structures. The number of atoms corresponds to the rhombohedral FCC primitive cell of the structure containing 99 atoms.

N^0	Site →	1 to 9	14	12			10/11/13	
	Structure	Mg	Mg	Mg	Pd	Ni	Pd	Ni
6	$Mg_{348}Ni_{48}$.cF412	82	1	4	0	0	0	12
7	$Mg_{348}Pd_{48}$.cF412	82	1	4	0	0	12	0
8	$Mg_{344}Pd_{48}$.cF412	82	0	4	0	0	12	0
9	$Mg_{344}Pd_{52}$.cF412	82	1	3	1	0	12	0
10	$Mg_{340}Pd_{52}$.cF412	82	0	3	1	0	12	0
11	$Mg_{340}Pd_{56}$.cF412	82	1	2	2	0	12	0
12	$Mg_{336}Pd_{56}$.cF412	81[a]	1	2	2[b]	0	12	0
13	$Mg_{336}Pd_{60}$.cF412	82	1	1	3	0	12	0
14	$Mg_{332}Pd_{64}$.cF412	82	1	0	4	0	12	0
19	$Mg_{344}Pd_{28}Ni_{24}$.cF412	82	1	2	2	0	6	6[c]
20	$Mg_{340}Pd_{32}Ni_{24}$.cF412	82	1	3	1	0	6	6[c]
21	$Mg_{348}Pd_{32}Ni_{16}$.cF412	82	1	4	0	0	8	4[d]
22	$Mg_{348}Pd_{32}Ni_{16}$.cF412	82	1	4	0	0	8	4[e]
23	$Mg_{348}Pd_{32}Ni_{16}$.cF412	82	1	4	0	0	8	4[f]

[a] A Mg vacant in site 1.
[b] Different supercell than N^0 8.
[c] Equal distribution of Ni and Pd between the three sites.
[d] 4 Ni atoms in site 10.
[e] 4 Ni atoms in site 11.
[f] 4 Ni atoms in site 13.

According to our calculations, the stable compound in the Mg_6Pd phase is that with the maximum Mg content (N^0 7), although other structures (N^0 8, 9, 11, 13, 14) are rather close in energy (less than 0.12 kJ/mol-atom). Taking into account the precision of our calculations, ~0.1 kJ/mol-atom, we cannot be certain of the composition of the stable compound at 0 K. However, these results predict the development of a homogeneity range at finite temperature as it has been experimentally observed [38].

3.1.4. Pseudo-binary formation enthalpies

The calculated pseudo-binary Mg_6(Pd−Ni) structures are displayed at the bottom part of Tables 1 and 2 (N^0 19 to 23). N^0 19 and 20 correspond to structures similar in composition and site occupancy, although not exactly equal, to that described experimentally [11]. On the other hand, N^0 21, 22 and 23 correspond to structures in which Ni fully replaces Pd in the sites 10, 11 and 13, respectively. The row N^0 6 in Tables 1 and 2 corresponds to the Mg_6Ni phase for which full Ni for Pd substitution takes place. See Table 2 for details of the Ni for Pd substitution. Fig. 1c gives $\Delta_f H_0$ for structures along pseudo-binary sections for three different Pd + Ni atomic fraction values. The solid lines are the tie-lines along the sections. Substitution of Pd by Ni drastically increases the enthalpy of formation of Mg_6(Pd−Ni) IMCs which ranges from −22.73 kJ/mol-atom (N^0 7, $Mg_{348}Pd_{48}$.cF412) to −6.60 kJ/mol-atom (N^0 6, $Mg_{348}Ni_{48}$.cF412). This is also in agreement with the stronger interaction of Mg with Pd than with Ni. The ΔE values are slightly larger for the Mg_6Ni type compound than for the pseudo-binaries, at least for the calculated structures.

Fig. 2 displays the Mg−Pd−Ni ternary phase diagram at the Mg-rich corner at $T = 0$ K emerging from DFT calculations. Black squares stand for stable compounds while open and grey squares stand for the unstable ones, being the latter ones less unstable. Lines connect stable compounds forming the convex hull. Two tie-triangles are defined by Mg.hP2−Mg_2Ni.hP18−$Mg_{348}Pd_{48}$.cF412 ($\epsilon + \beta + \rho$) and $Mg_{348}Pd_{48}$.cF412−Mg_2Ni.hP18−$Mg_{57}Pd_{13}$.cP140 ($\beta + \rho + \gamma$) phases. No stable ternary compound is found at $T = 0$ K in the Mg−Mg_2Ni−Mg_6Pd corner.

This is in contrast with experimental results recently published [11–14] that show unambiguously that pseudo-binary Mg_6(Pd−Ni) compounds, with a fraction of Ni for Pd substitution up to 75%, are stable at finite temperatures (673 K). Taking into account that the energy distances to the convex hull of the calculated structures are not very high, we speculate that stabilisation of the ternary compounds could be driven by entropic effects. In order to show that finite temperature effects are indeed responsible for the stability of the compounds, we have estimated such effects by the method outlined above. The results will be discussed in section 3.2.

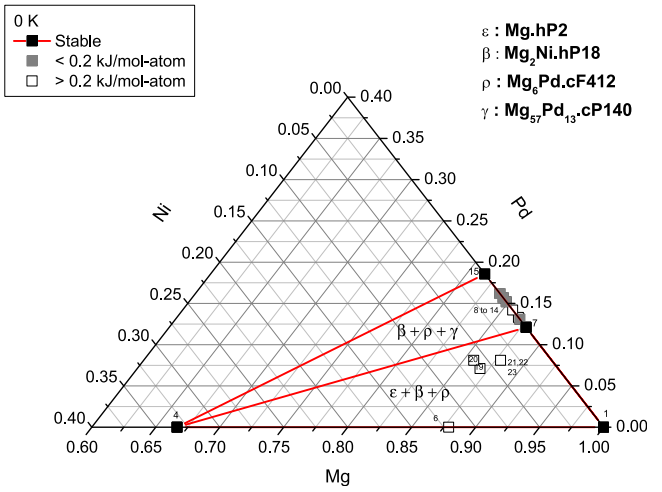

Fig. 2. Mg−Pd−Ni ternary phase diagram at $T = 0$ K at the Mg-rich corner. Black squares stand for stable phases connected by solid lines forming the convex hull. Grey squares and open squares represent unstable structures with a distance to the convex hull lower and higher respectively than 0.2 kJ/mol-atom.

3.1.5. Site occupancy of Ni in the pseudo-binary compounds

The three structures N^0 21, 22 and 23 were studied with the purpose of discussing the site occupancy of Ni in the pseudo-binary compounds. In these structures, full replacement of Pd atoms in a specified site was allowed. Even though such a distribution of Ni is unrealistic and all of them are unstable, it allows a meaningful comparison of the energetics associated to the different sites. The ΔE value is the smallest one when Ni occupies site 11, followed by site 13 and then site 10. We have also investigated the placement of Ni in site 12, but in this case ΔE is even higher, and that situation is not directly comparable to the previous one as Ni would not only substitute for Pd but also for Mg. The sequence of Ni preference

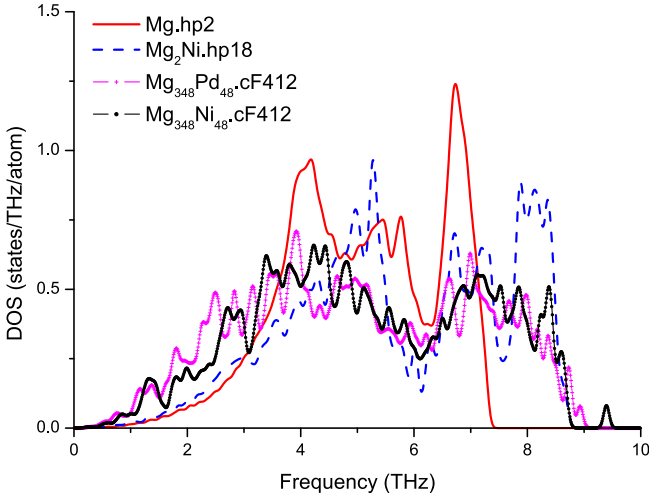

Fig. 3. Phonon DOS normalised to three per atom for Mg.hp2, Mg_2Ni.hp18, $Mg_{348}Pd_{48}$.cF412 and $Mg_{348}Ni_{48}$.cF412.

sites, 11, 13, 10 and 12 is in perfect agreement with the results obtained from neutron diffraction experiments [11]. In this experimental work, the fractional occupation of Ni in sites 11, 13, 10 and 12 was determined to be 0.60, 0.44, 0.36 and 0.04, respectively. This sequence is related to the site volume, which increases with the coordination number (CN), and the relative atomic radii of Ni and Pd elements. Thus, Ni, the smallest element prefers sites with low CN, like site 11 which has 10 neighbours, whereas Pd, the largest element, prefers sites with high CN, as happens with site 12 which has 13 neighbours.

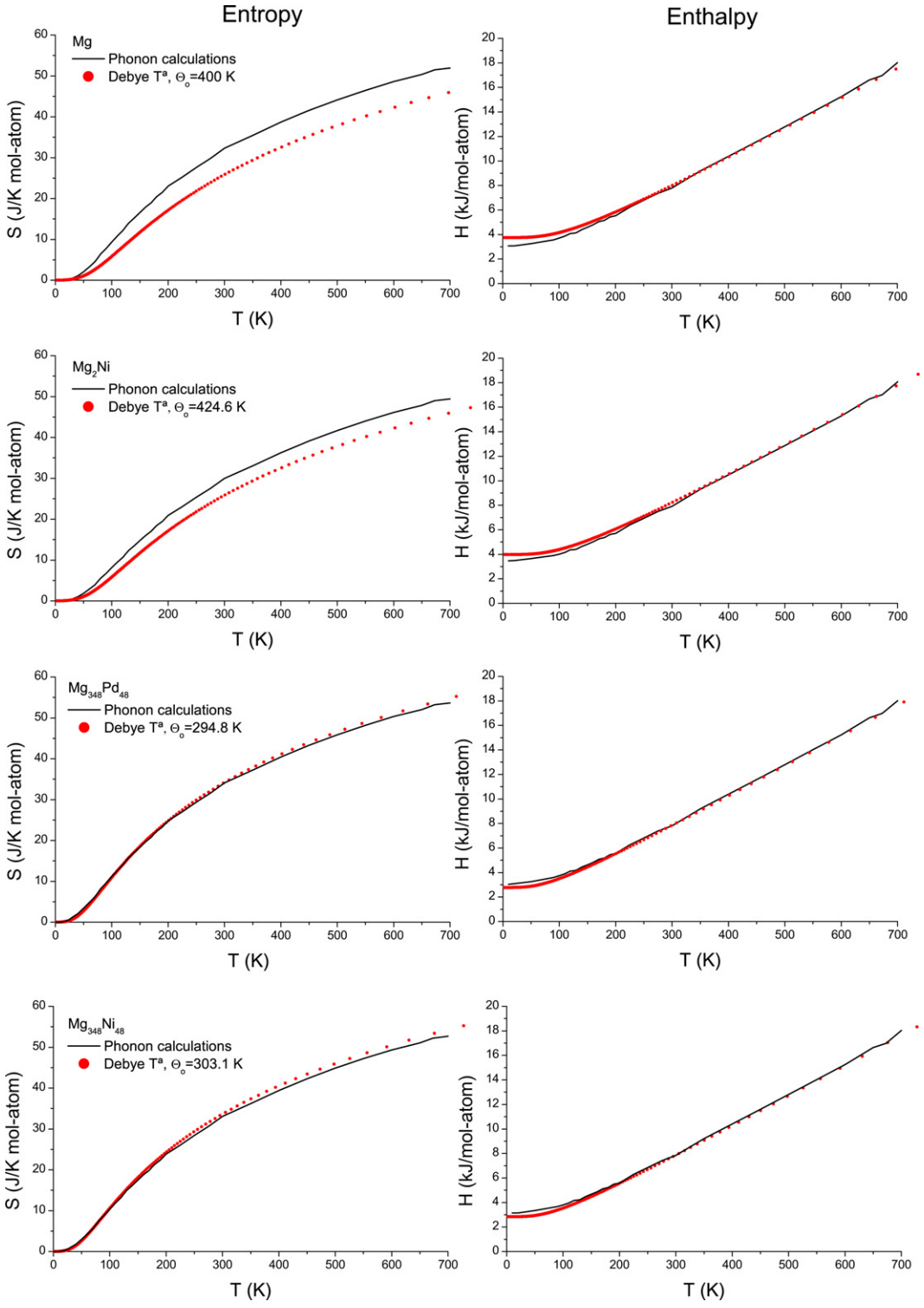

Fig. 4. High temperature vibrational enthalpy and entropy obtained in the harmonic approximation from the phonon DOS (solid line) compared to those obtained from the Debye temperatures (circles).

Please cite this article in press as: Fernandez JF, et al., First-principles phase stability calculations and estimation of finite temperature..., Intermetallics (2010), doi:10.1016/j.intermet.2010.11.024

3.2. Finite temperature thermodynamics

3.2.1. Comparison between Debye model and phonon calculations

Fig. 3 shows the calculated phonon DOS normalised to three per atom for Mg.hp2, Mg_2Ni.hp18, $Mg_{348}Pd_{48}$.cF412 and $Mg_{348}Ni_{48}$.cF412. For Mg.hp2 very good agreement with experimental data [40] and previous calculations [49] is found. For the other compounds, as far as we know, there is no data for comparison. The phonon DOS for the cubic compounds are quite similar indicating little effect of the Ni for Pd substitution in the vibrational properties. In particular, from these results, we would expect similar Debye temperatures for the pseudo-binaries and then very similar thermodynamic vibrational behaviour at high temperatures.

Fig. 4 shows the calculated high temperature vibrational enthalpy and entropy obtained in the harmonic approximation from the phonon DOS for the four compounds (solid lines). They are compared with estimates (circles) based on the properties derived from Ref. [50] (Mg.hp2) or with estimates obtained from Debye temperatures calculated in this work (Mg_2Ni.hp18, $Mg_{348}Pd_{48}$.cF412 and $Mg_{348}Ni_{48}$.cF412, see Section 3.2.2). In order to compare both sets of curves, the zero-point vibrational energy (9/8 Rθ_0 [36]) has been added to the Debye free energy. The enthalpy curves calculated by the two methods are in very good agreement for the four compounds. As for the entropy, the agreement is also very good for the $Mg_{348}Pd_{48}$.cF412 and $Mg_{348}Ni_{48}$.cF412 compounds. For Mg_2Ni.hp18, the discrepancy in the entropy values at 673 K obtained from both methods is only of 7%. The worst agreement is obtained for the Mg.hp2 with a discrepancy in the entropy values at 673 K of around 10%. Debye temperature for the elements, Mg, Ni and Pd, were taken from Ref. [50], suggesting that in the case of Mg, the θ_0 value quoted there is slightly overestimated. From those results we safely conclude that the method presented in this work is reliable enough to examine the high temperature phase diagram for the complex compounds of this study.

3.2.2. Phase stability at finite temperatures

Table 3 gives the values of parameters used to calculate the finite temperature thermodynamics of the compounds. We give B_0 at $T = 0$ K, θ_0, and the thermodynamic properties at $T = 673$ K derived from them in the harmonic approximation (see Table 3 caption for an explanation of the several thermodynamic properties listed). B_0 and θ_0 for the elements have been obtained from Ref. [50].

The values of B_0 and θ_0 for all IMCs are rather similar. No experimental data has been found in the literature for comparison. Also the specific heat and the vibrational contribution to enthalpy and entropy are quite similar for all IMCs, being closer to elemental Pd than to elemental Mg or Ni. There is a general tendency of decreasing C_v, $H^h_{673} - H_0$ and S^h_{673} when Ni gradually substitutes Pd. On the other hand, the S^{conf} shows more differences between compounds. This term comes from substituting Ni for Pd and Pd for Mg and it is maximal for the $Mg_{344}Pd_{28}Ni_{24}$.cF412 structure (N^0 19).

$\Delta_f H_{673}$ increases by less than 1 kJ/mol-atom as compared to $T = 0$ K value, reflecting the negligible contribution of vibrations to the enthalpy of formation of these compounds. On the other hand, the $\Delta_f S_{673}$ is positive for most of the compounds, tending to stabilising them. The larger stabilising effect is for the pseudo-binary structures N^0 19 and 20, which exhibit the largest contribution from configurational entropy.

The evolution with T of the Gibbs free energy of formation for $Mg_{344}Pd_{28}Ni_{24}$.cF412 (solid squares) and $Mg_{348}Ni_{48}$.cF412 (solid circles) compounds are compared in Fig. 5 to the corresponding one for phase separation (empty squares and circles, respectively). The pseudo-binary becomes stable at a lower T (~100 K) than the binary (~200 K). Note that the stability against decomposition for both compounds increase with T, although, it should be mentioned that the model is less accurate at high temperatures due to anharmonic effects.

To summarize, we have calculated the formation Gibbs free energy at 673 K for all studied compounds and redrawn the phase diagram at the Mg-rich corner (Fig. 6). The same symbols as in Fig. 2 are used. A new feature appears in the phase diagram, namely a single phase field extending from the binary Mg_6Pd phase to the Mg_6Ni compound. The pseudo-binary structures, N^0 19 and 20 (with compositions close to that experimentally studied in Ref. [11]) become stable.

We do predict the binary $Mg_{348}Ni_{48}$ compound as stable, in contrast to the experimental fact that the compound is only formed during rapid solidification from the melt [22] in a metastable state that transforms to a Mg + Mg_2Ni mixture after heating above 473 K. Fig. 5 indicates that, according to our calculations, the compound is

Table 3
Bulk modulus at $T = 0$ K, B_0, Debye temperature, θ_0, constant volume specific heat at 673 K, C_v, the vibrational contribution at 673 K to enthalpy, $H^h_{673} - H_0$, and entropy, S^h_{673}, the configurational entropy, S^{conf}, and the enthalpy, entropy and Gibbs free energy of formation at 673 K, $\Delta_f H_{673}$, $\Delta_f S_{673}$ and $\Delta_f G_{673}$, respectively, for the several compounds involved in the finite temperature calculations.

N^0	Compound	B_0 (GPa)	θ_0 (K)	$C^h_{v,673}$ (J/K mol-atom)	$H^h_{673} - H_0$ (kJ/mol-atom)	S^h_{673} (J/K mol-atom)	S^{conf} (J/K mol-atom)	$\Delta_f H_{673}$ (kJ/mol-atom)	$\Delta_f S_{673}$ (J/K mol-atom)	$\Delta_f G_{673}$ (kJ/mol-atom)
1	Mg.hp2	35.4[a]	400.0[a]	24.53	13.34	46.44	0	0	0	0
2	Pd.cF4	181[a]	274 .0[a]	24.80	14.37	55.77	0	0	0	0
3	Ni.cF4	186[a]	450 .0[a]	24.41	12.95	43.56	0	0	0	0
4	Mg_2Ni.hP18	71.5	424.6	24.47	13.15	45.04	0	−19.34	−0.44	−19.04
6	$Mg_{348}Ni_{48}$.cF412	47.2	303.1	24.74	14.13	53.28	0	−5.76	7.19	−10.60
7	$Mg_{348}Pd_{48}$.cF412	53.3	294.8	24.76	14.20	53.96	0	−21.99	6.39	−26.95
8	$Mg_{344}Pd_{48}$.cF412	53.2	294.4	24.76	14.20	53.96	0	−22.17	6.38	−26.46
9	$Mg_{344}Pd_{52}$.cF412	54.8	295.2	24.76	14.20	53.96	1.17	−23.80	7.46	−28.82
10	$Mg_{340}Pd_{52}$.cF412	54.5	294.2	24.76	14.20	53.96	1.17	−23.34	7.45	−28.35
11	$Mg_{340}Pd_{56}$.cF412	56.4	295.6	24.75	14.19	53.89	1.44	−25.62	7.57	−30.71
12	$Mg_{336}Pd_{56}$.cF412	56.2	294.7	24.76	14.20	53.96	1.44	−24.68	7.63	−29.81
13	$Mg_{336}Pd_{60}$.cF412	58.2	296.3	24.75	14.19	53.89	1.17	−27.41	7.21	−32.26
14	$Mg_{332}Pd_{64}$.cF412	59.9	296.8	24.75	14.18	53.79	0	−29.16	5.84	−33.09
15	$Mg_{57}Pd_{13}$.cP140	64.0	298.1	24.75	14.17	53.69	0	−33.61	5.52	−37.32
19	$Mg_{344}Pd_{28}Ni_{24}$.cF412	51.2	297.7	24.75	14.17	53.72	5.49	−15.72	12.29	−23.99
20	$Mg_{340}Pd_{32}Ni_{24}$.cF412	52.9	298.3	24.75	14.17	53.67	5.76	−17.53	12.41	−25.88
21	$Mg_{348}Pd_{32}Ni_{16}$.cF412	51.0	296.7	24.75	14.18	53.79	0	−16.33	6.71	−20.84
22	$Mg_{348}Pd_{32}Ni_{16}$.cF412	51.0	297.2	24.75	14.18	53.79	0	−16.71	6.71	−21.22
23	$Mg_{348}Pd_{32}Ni_{16}$.cF412	51.0	296.9	24.75	14.18	53.79	0	−16.41	6.71	−20.92

[a] Ref. [50].

Please cite this article in press as: Fernandez JF, et al., First-principles phase stability calculations and estimation of finite temperature..., Intermetallics (2010), doi:10.1016/j.intermet.2010.11.024

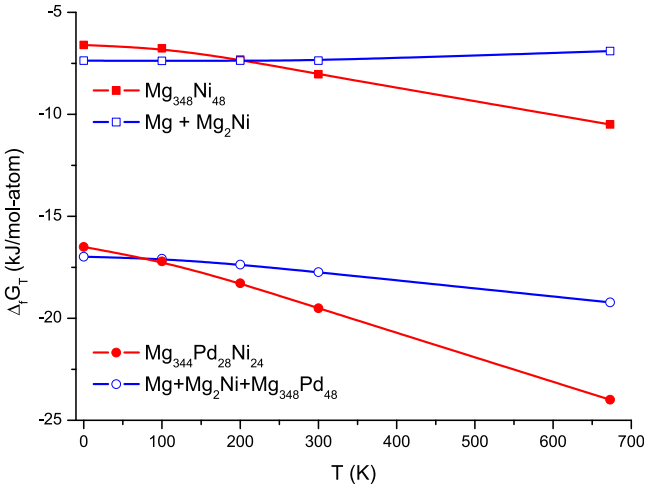

Fig. 5. Evolution with T of the Gibbs free energy of formation. Solid square and circles corresponds to $Mg_{344}Pd_{28}Ni_{24}$.cF412 and $Mg_{348}Ni_{48}$.cF412 compounds, respectively. Empty symbols stand for the corresponding $\Delta_f G_T$ for phase separation at the same atomic composition.

still stable at 673 K. The Gibbs free energy of formation at 673 K of $Mg_{348}Ni_{48}$.cF412 is −10.60 kJ/mol-atom, i.e., −3.68 kJ/mol-atom below the tie-triangle formed by Mg–Mg_2Ni–Mg_6Pd phases.

Another interesting feature observed in Fig. 6 is the homogeneity range for the binary Mg_6Pd phase. The Mg concentrations at the limits of the homogeneity range are 87.9 at % Mg and 84.8 at % Mg, in very good agreement with experimental data [38].

We have recently studied the homogeneity range and crystal structure of Mg_6(Pd, Ni) pseudo-binaries by chemical and structural methods [14]. According to our results the solubility limit at 673 K attains 9 at.% Ni, i.e., more than four times the value previously reported [15]. This corresponds to a degree of Ni for Pd substitution close to 75%. From these results it was claimed that the Mg–Pd–Ni phase diagram at the Mg-rich corner should be revised. The solid thin line (blue online) in Fig. 6 corresponds to the proposed modification of the phase diagram according to the composition of pseudo-binary Mg_6(Pd, Ni) compounds (blue dots online) determined in the experimental work. As can be seen the results we present here are in very good agreement with the proposed modification of the ternary phase diagram.

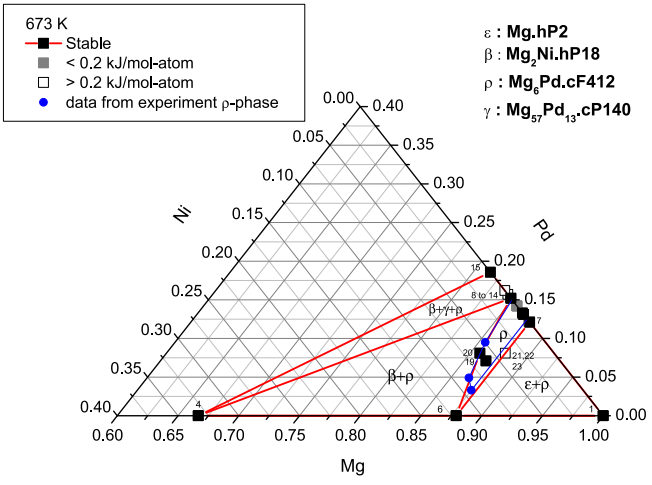

Fig. 6. Same as Fig. 2 at T = 673 K. Dots and solid line (blue online) are respectively, experimental data and the proposed modification of the phase diagram [14] (For interpretation of the reference to colour in this figure legend, the reader is referred to the web version of this article).

As a final remark, we would like to emphasize that the present calculations concern very complex compounds such as pseudo-binary $Mg_6(Pd_xNi_{1-x})$ IMCs with almost 100 atoms in the primitive cell. Despite of this demanding scenario, our results describe with good accuracy the phase diagram of the ternary Mg–Pd–Ni system at the Mg-rich corner. Therefore, we believe that the combination of DFT calculations with thermodynamic modelling of finite temperature effects is a valid approach to determine ternary phase diagrams with complex phases like the one studied here.

4. Conclusions

DFT calculations show that at T = 0 K the stable compounds at the Mg-rich corner (>80 at.% Mg) of the Mg–Pd–Ni phase diagram are Mg.hP2, Mg_2Ni.hP18, $Mg_{348}Pd_{48}$.cF412 and $Mg_{57}Pd_{13}$.cP140 phases. No pseudo-binary stable compounds are found. At finite temperature, T = 673 K, we have found that the binary Mg_6Pd phase extends into a large ternary Mg_6(Pd, Ni) region. In particular, the pseudo-binary structures, $Mg_{344}Pd_{28}Ni_{24}$.cF412, $Mg_{344}Pd_{28}Ni_{24}$.cF412 with Pd and Ni atomic concentrations similar to the compounds studied experimentally become stable. Vibrational and configurational entropic effects are responsible for the finite temperature stability of the pseudo-binaries. Our calculations also show that the $Mg_{348}Ni_{48}$.cF412 structure is stable at 673 K in contrast to experiments showing that this compound is metastable. As regards Ni for Pd substitution, we have found that Ni substitutes Pd preferentially in site 11 following by site 13, 10 and 12, a sequence which is in perfect agreement with the experimental findings.

Acknowledgements

Some of the authors thank the Spanish Minister of Education and Science, MICINN, for financial support under contract No. MAT2008-06547-C02-01.

References

[1] Zuttel A. Mater Today 2003;6:24.
[2] Fernández JF, Sánchez C. J Alloys Compd 2002;340:189–98.
[3] Bogdanović B, Bohmhammel K, Christ B, Reiser A, Schlichte K, Vehlen R, et al. J Alloys Compd 1999;282:84–92.
[4] Reilly JJ, Wiswall RH. Inorg Chem 1968;7(11):2254–6.
[5] Didisheim JJ, Zolliker P, Yvon K, Fischer P, Schefer J, Gubelmann M, et al. Inorg Chem 1984;23(13):1953.
[6] Zolliker P, Yvon K, Fischer P, Schefer J. Inorg Chem 1985;24(24):4177.
[7] Reilly JJ, Wiswall RH. Inorg Chem 1967;6(12):2220–3.
[8] Mintz MH, Gavra Z, Kimmel G, Hadari Z. J Less Common Met 1980;74:263–70.
[9] Saunders N, Miodownik AP. CALPHAD (calculation of phase diagrams): a comprehensive guide. New York: Pergamon; 1998.
[10] Lukas HL, Fries SG, Sundman B. Computational thermodynamics. Cambridge University Press; 2007.
[11] Cuevas F, Fernández JF, Ares JR, Leardini F, Latroche M. J Solid State Chem 2009;182:2890–6.
[12] Fernández JF, Ares JR, Cuevas F, Bodega J, Leardini F, Sánchez C. Intermetallics 2010;18:233–41.
[13] Fernández JF, Cuevas F, Leardini F, Bodega J, Ares JR, Garces G, et al. J Alloys Compd 2010;495:663–6.
[14] Cuevas F, Fernández JF, Ares JR, Leardini F, Sánchez C. J Phys Chem Solids 2010;71(9):1259–63.
[15] Gupta KP. J Phase Equilib Diffus 2004;25:191–4.
[16] Bonhomme F, Yvon K. J Alloys Compd 1995;227:L1–3.
[17] Samson S. Acta Crystallogr 1972;B28:936.
[18] Ferro R, Rambaldi G. J Less Common Met 1960;2:383.
[19] Westin L, Edshammar LE. Acta Chem Scand 1971;25:1480.
[20] Westin L, Edshammar LE. Chem Scr 1973;3:15.
[21] Kamegawa A, Goto Y, Kataoka R, Takamura H, Okada M. Renew Energ 2008;33:221–5.
[22] Kempen ATW, Nitsche H, Sommer F, Mittemeijer EJ. Metall Mater Trans A 2002;33A:1041–50.
[23] Teresiak A, Uhlemann M, Thomas J, Gebert A. J Alloys Compd 2009; 475(1–2):191–7.
[24] Kresse G, Hafner J. Phys Rev B 1993;47:RC558.

[25] Kresse G, Furthmuller J. Phys Rev B 1996;54:11169.
[26] Blöchl P. Phys Rev B 1994;50:17953.
[27] Kresse G, Joubert D. Phys Rev B 1999;59:1758.
[28] Perdew JP, Chevary JA, Vosko SH, Jackson KA, Pederson MR, Singh DJ, et al. Phys Rev B 1992;46:6671–87.
[29] Mihalkovič M, Widom M. Phys Rev B 2004;70:144107.
[30] M. Mihalkovič, M. Widom, http://alloy.phys.cmu.edu/.
[31] Siethoff H. Intermetallics 1997;5:625–32.
[32] Siethoff H, Ahlborn K. Phys Stat Sol B 1995;190:179.
[33] Siethoff H, Ahlborn K. J Appl Phys 1996;79:2968.
[34] Li C, Wu P. Chem Mater 2001;13:4642–8.
[35] Li C, Chin YL, Wu P. Intermetallics 2004;12:103–9.
[36] Moruzzi VL, Janak JF, Schwarz K. Phys Rev B 1988;37(2):790–9.
[37] Chen Q, Sundman B. Acta Mater 2001;49:947–61.
[38] Makongo JPA, Prots Y, Burkhardt U, Niewa R, Kudla C, Kreiner G. Philos Mag 2006;86:427–33.
[39] Kresse G, Furthmuller J, Hafner J. Europhys Lett 1995;32:729–34.
[40] Pynn R, Squires GL. Proc R Soc Lond A 1972;326:347–60.
[41] van Walle A, Ceder G. Rev Mod Phys 2002;74:11.
[42] Makongo JPA, Kudla C, Prots Yu, Niewa R, Burkhardt U, Kreiner G. Z. Kristallogr. NCS 2005;220:289–90.
[43] Hlukhyy V, Pöttgen P. Intermetallics 2004;12:533–7.
[44] Huot J, Yonkeu A, Dufour J. J Alloys Compd 2009;475(1–2):168–72.
[45] Okamoto H. Phase diagrams for binary alloys. USA: ASM International; 2000.
[46] van Setten MJ, de Wijs GA, Brocks G. Phys Rev B 2007;76:075125.
[47] Broedersz CP, Gremaud R, Dam B, Griessen R, Løvvik OM. Phys Rev B 2008;77:024204.
[48] Deng Y, Wang T, Zhang W, Tang B, Zeng X, Ding W. Trans Nonferrous Met Soc China 2008;18:416–20.
[49] Arroyave R, Liu Z-K. Phys Rev B 2006;74:174118.
[50] Kittel C. Introduction to solid state physics. 7th ed. New York: John Wiley and Sons, Inc.; 1996.

Please cite this article in press as: Fernandez JF, et al., First-principles phase stability calculations and estimation of finite temperature..., Intermetallics (2010), doi:10.1016/j.intermet.2010.11.024